iScience

Article

Loss of function of *Atrx* recapitulates phenotypes of alternative lengthening of telomeres in a primary mouse model of sarcoma

Graphical abstract

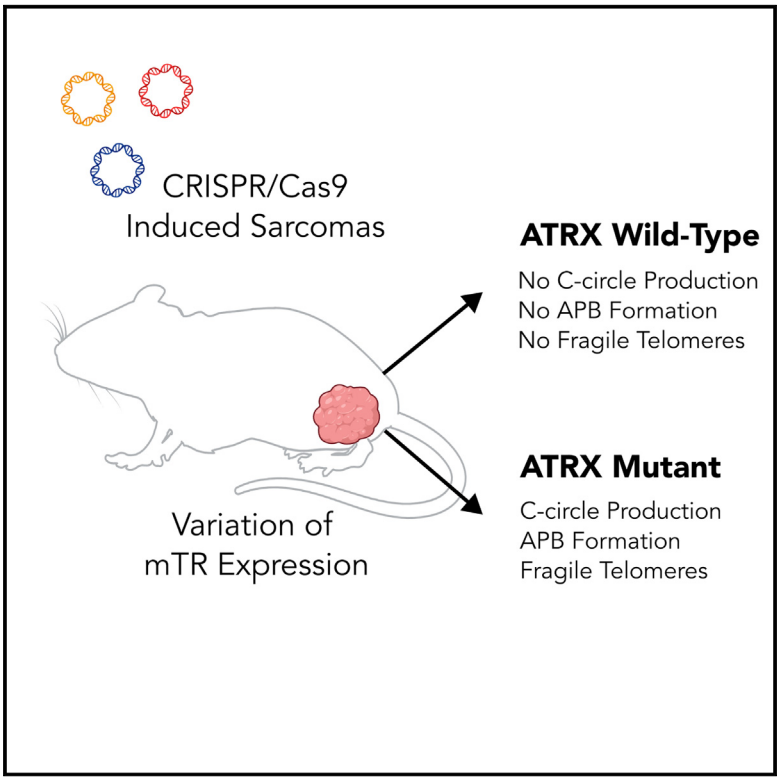

Authors

Matthew Pierpoint, Warren Floyd, Amy J. Wisdom, ..., Brendan C. Dickson, Matthew S. Waitkus, David G. Kirsch

Correspondence

david.kirsch@uhn.ca

In brief

Molecular biology; Cell biology; Cancer

Highlights

- A primary mouse model of sarcoma with conditional knockout of *Atrx* and mTR
- Tumors with loss of *Atrx* display multiple molecular phenotypes of ALT

Pierpoint et al., 2025, iScience *28*, 112357
May 16, 2025
https://doi.org/10.1016/j.isci.2025.112357

CellPress

iScience

CellPress
OPEN ACCESS

Article

Loss of function of *Atrx* recapitulates phenotypes of alternative lengthening of telomeres in a primary mouse model of sarcoma

Matthew Pierpoint,[1,2,13] Warren Floyd,[3,13] Amy J. Wisdom,[4] Lixia Luo,[5] Yan Ma,[5] Brendan C. Dickson,[6,7] Matthew S. Waitkus,[8,9,10] and David G. Kirsch[1,2,5,11,12,14,*]

[1]Duke Department of Pharmacology and Cancer Biology, Duke University Medical Center, Durham, NC 27710, USA
[2]Radiation Medicine Program, Princess Margaret Cancer Centre, Toronto, ON M5G 2M9, Canada
[3]Department of Radiation Oncology, University of Texas MD Anderson Cancer Center, Houston, TX, USA
[4]Harvard Radiation Oncology Program, Boston, MA 02115, USA
[5]Duke Department of Radiation Oncology, Duke University Medical Center, Durham, NC 27710, USA
[6]Department of Pathology and Laboratory Medicine, Mount Sinai Hospital, Toronto, ON, Canada
[7]Laboratory Medicine and Pathobiology, University of Toronto, Toronto, ON, Canada
[8]Duke Cancer Institute, Duke University School of Medicine, Durham, NC 27710, USA
[9]Department of Neurosurgery, Duke University School of Medicine, Durham, NC 27710, USA
[10]The Preston Robert Tisch Brain Tumor Center at Duke, Durham, NC 27710, USA
[11]Department of Radiation Oncology, University of Toronto, Toronto, ON M5G 2M9, Canada
[12]Department of Medical Biophysics, University of Toronto, Toronto, ON M5G 2M9, Canada
[13]These authors contributed equally
[14]Lead contact
*Correspondence: david.kirsch@uhn.ca
https://doi.org/10.1016/j.isci.2025.112357

SUMMARY

The development of a telomere maintenance mechanism is essential for immortalization in human cancer. While most cancers elongate their telomeres by expression of telomerase, 10–15% of human cancers utilize a pathway known as alternative lengthening of telomeres (ALT). ALT is commonly associated with loss-of-function mutations in ATRX. Here, we developed a genetically engineered primary mouse model of sarcoma in CAST/EiJ mice to investigate the extent to which telomerase deficiency and Atrx-inactivation lead to ALT induction. We observed increases in multiple ALT-associated phenotypic indicators in tumors with loss of function mutations of *Atrx*. Furthermore, we found that loss of *Atrx* leads to an increase in telomeric instability and telomere sister chromatid exchange. However, Atrx-deficient tumors did not show productive telomere length maintenance in the absence of telomerase. This primary mouse model of sarcoma could facilitate future investigations into the molecular features of ALT *in vivo*.

INTRODUCTION

Telomeres are hexanucleotide repetitive elements that are highly conserved to provide stability to the ends of linear chromosomes.[1] During the process of cell division, telomeres are incompletely replicated leading to their progressive shortening, and this is known as the end-replication problem.[2] To achieve replicative immortality, most cancers maintain telomere length by activating a mechanism of telomere maintenance, thus preventing telomere erosion and telomere crisis. It is estimated that 85% of cancers maintain telomeres via the activation of canonical telomerase activity. However, approximately 10–15% of cancers use alternative mechanisms, collectively termed alternative lengthening of telomeres (ALT), to maintain their telomeres.[3,4] Phenotypic markers of ALT in mammalian cells include abnormally long and heterogeneous telomere length, ALT-associated promyelocytic leukemia bodies (APBs), extrachromosomal telomeric c-circles, and increased frequency of telomere sister chromatid exchange.[4–7]

Thus far, the genomic determinants of ALT have not been fully elucidated, but the activation of ALT has been strongly correlated with the loss of α-thalassemia/mental retardation, X-linked (ATRX) protein function or expression in multiple subtypes of sarcoma including osteosarcoma, leiomyosarcoma, dedifferentiated liposarcoma, pleomorphic liposarcoma, angiosarcoma, myxofibrosarcoma, and undifferentiated pleomorphic sarcoma.[8–13] In these sarcoma subtypes, the presence of ALT and ATRX loss correlates with shorter progression-free survival and worse overall survival[14]. *In vitro* studies have shown that the loss of ATRX in human cells can lead to the development of ALT while reintroducing ATRX expression can repress ALT activity, highlighting its regulatory role in telomere dynamics.[15–20] Importantly, ATRX is one of the most frequently mutated genes in ALT positive cancers, and previous work has demonstrated

that the loss of ATRX leads to telomere dysfunction.[21,22] While the mutation of ATRX is correlated with the activation of ALT in sarcomas, some ALT positive cancers retain functional ATRX, suggesting that there are multiple pathways for the activation of ALT.[23]

Murine telomerase function is analogous to that of human telomerase, with a mouse telomerase RNA (mTR) serving as an RNA template for the mouse telomerase reverse transcriptase gene (mTERT). This template enables reverse transcription of telomeres. However, in contrast to human biology, mice have significantly longer telomeres and have been shown to express telomerase in normal tissues.[24] Despite the prevalence of ALT activation in human cancer, to our knowledge, efforts to recapitulate ALT in primary mouse models of cancer have been largely unsuccessful. Additionally, previous studies have demonstrated that, unlike in human cells, telomere maintenance is not essential for the oncogenic transformation of murine cells, independent of their telomere length.[25] CAST/EiJ mice have been used to study telomere shortening after loss of telomerase because they have shorter telomeres compared to commonly used 129/SVJ and C57BL/6 laboratory mouse strains.[26] Studies using CAST/EiJ mice with and without genetic loss of mTR have shown that they are able to recapitulate phenotypes of telomere shortening observed in human diseases when telomerase function is lost and that the shortening of telomeres by loss of mTR leads to increased recombination events.[27,28] In this work, we generate and characterize a genetically engineered mouse model of soft tissue sarcoma which recapitulates multiple molecular markers of the ALT pathway after activation of oncogenic *Kras* and loss of function mutations in both *Trp53* and *Atrx*.

RESULTS

A CRISPR/Cas9 primary model of sarcoma in CAST/EiJ mice

For this study, we generated mice with constitutively expressed Cas9 (Rosa26-1loxp-Cas9) either with or without functional mTR alleles on a CAST/EiJ genetic background.[25,29] To initiate primary tumors in these mice, we designed a two-plasmid system to activate oncogenic $Kras^{G12D}$ and induce the loss of function of either *Trp53* (CAST KP model) or *Trp53* and *Atrx* (CAST KPA model). In this model, intramuscular injection and electroporation of plasmids into the right hindlimb of mice leads to the formation of spatially and temporally restricted soft tissue sarcomas after approximately 60 days, which is similar to previously published models[30,31] (Figure 1A). The first plasmid activates oncogenic $Kras^{G12D}$ using homology-directed repair, and the second plasmid contains single guide RNAs (sgRNAs), which induce insertion/deletion (indel) mutations to either *Trp53* alone or *Trp53* and *Atrx*.

To determine the genomic status of *Atrx* after CRISPR/Cas9 editing, we performed targeted next-generation amplicon sequencing of tumor tissue to evaluate the mutation status of each tumor for *Atrx*. All CAST KP tumors sequenced consisted entirely of wild-type *Atrx* sequences. Out of 21 CAST KPA tumors, 14 contained either frameshift or large deletion mutations in *Atrx* (Figure 1B). To test if amplicon sequencing results matched protein expression, we performed immunohistochemistry for ATRX on tumor sections and found that tumors with *Atrx* loss of function mutations demonstrated a loss of nuclear staining in all but one case (Figures 1C–1E, Table S1). To confirm the loss of ATRX protein expression, we performed western blotting using primary cell lines and demonstrated the complete knockout of ATRX protein in the CAST KPA but not CAST KP cell lines (Figure S1). Because the loss of *Trp53* and activation of oncogenic $Kras^{G12D}$ is sufficient to drive tumorigenesis in mice, an additional loss of function mutation of *Atrx* is not required for tumor formation.[30] Therefore, tumors that retain expression of *Atrx* after non-frameshift mutations are classified in this work as CAST KPA* to denote the presence of non-frameshift mutations of *Atrx* and the likely retention of *Atrx* function.

Tumor sections were stained with hematoxylin and eosin (H&E) and a panel of immunohistochemical markers routinely used to classify human soft tissue sarcomas. The tumors exhibited a spindle to epithelioid cell morphology with moderate nuclear pleomorphism and brisk mitotic activity. The intervening stroma was variably myxoid, and areas of necrosis were common. Overall, the morphology was compatible with a high-grade soft tissue sarcoma. Immunohistochemical analysis revealed variable staining for desmin and smooth muscle actin; tumors less commonly expressed pan-cytokeratin, and there was rare immunoreactivity for myogenin. No apparent histologic or immunohistochemical differences were observed between tumors with and without mutations of *Atrx*, or between tumors with different expression of mTR. (Figure 2). Overall, the findings suggest mesenchymal neoplasms generated using this model represent high-grade sarcomas without a specific line of differentiation.

The telomere length distribution of tumors and normal liver controls was measured using the telomere restriction fragment (TRF) assay (Figure 3A). Interestingly no increase in telomere length heterogeneity or very long telomeres was observed when comparing *Atrx* deficient and *Atrx* wild type tumors, suggesting that *Atrx* knockout and mTR deletion are not by themselves sufficient for telomere lengthening. The telomerase repeated amplification protocol (TRAP assay) confirmed that $mTR^{+/+}$ and $mTR^{+/-}$ primary cell lines retained telomerase activity, and that $mTR^{-/-}$ has abrogated telomerase activity, as expected[32] (Figure 3B).

Assaying for alternative lengthening of telomeres in primary tumors

C-circles are partially single stranded circular telomeric DNAs found exclusively in ALT+ tumors and cell lines.[6] The c-circle assay quantifies ALT activity in cell lines and tumors using phi-29 rolling circle amplification and measures the resulting products by dot blot or qPCR techniques.[6] In this study, we measured c-circles within genomic DNA harvested from CAST KP, CAST KPA*, and CAST KPA fresh frozen tumors as well as ALT positive U2OS and telomerase positive 143B human cell line controls (Figures 4A and S2). When comparing the relative chemiluminescent signal of the dot blots across three replicates, the data indicate that the loss of *Atrx* function leads to a marked increase in c-circle formation in tumors, while non-frameshift mutations in Atrx do not lead to the production of c-circles (Figure 4B). Notably, *Atrx* inactivation led to the production of c-circles in

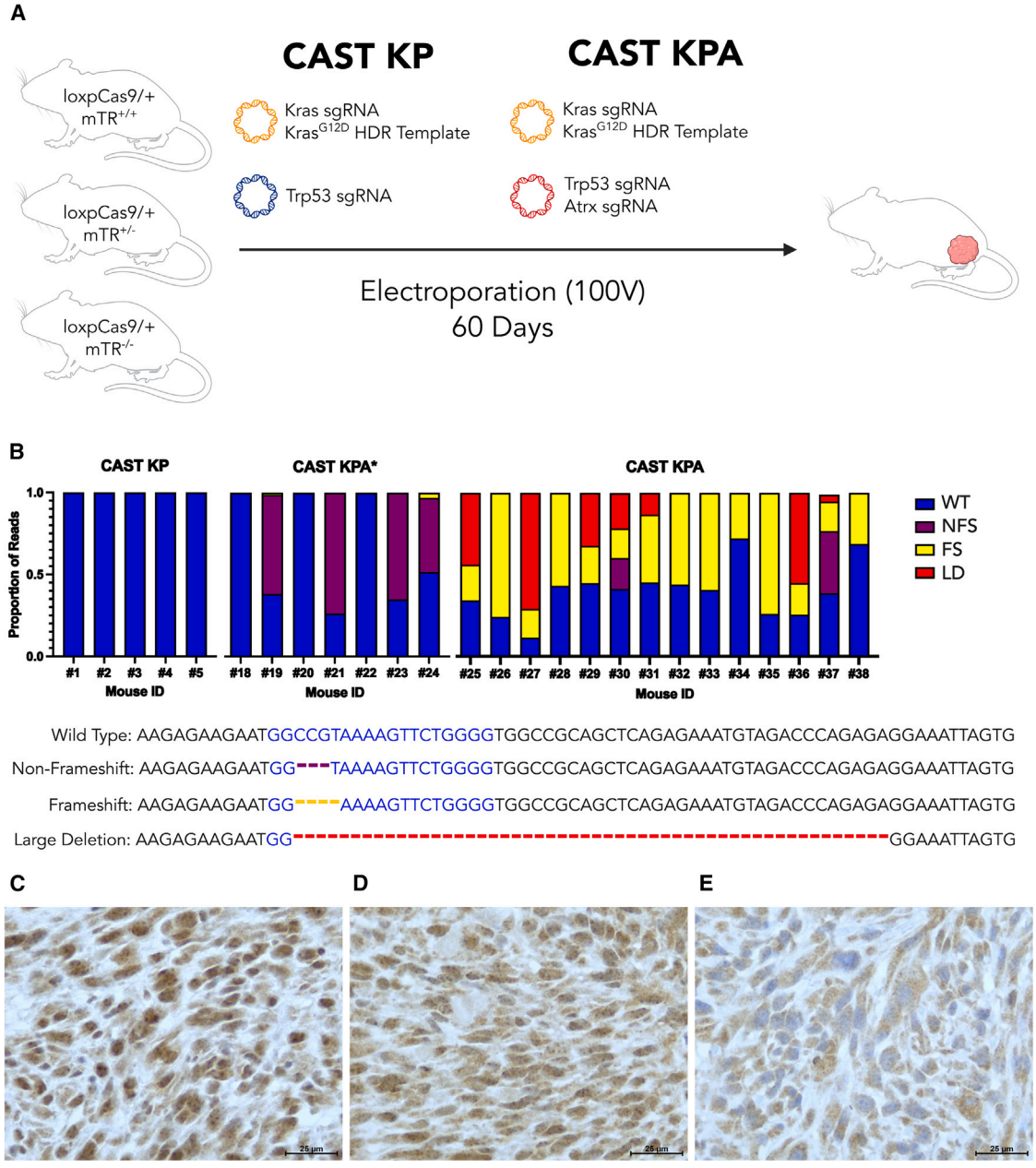

Figure 1. Genetically engineered mouse model of soft tissue sarcoma with loss of *Atrx*

(A) CAST/EiJ mice expressing Cas9 (Rosa26-1loxp-Cas9/+) and either wild type mTR (mTR$^{+/+}$), heterozygous mTR loss (mTR$^{+/-}$), or homozygous mTR loss (mTR$^{-/-}$) are injected in the gastrocnemius muscle with a two-plasmid system to induce expression of oncogenic *Kras*^{G12D} and biallelic mutation of *Trp53* (CAST KP model), with additional mutation of *Atrx* (CAST KPA model), followed by electroporation of the gastrocnemius muscle. Tumor initiation occurs approximately 60 days after electroporation of the plasmids.

(B) Graphical representation of the *Atrx* mutation profile generated from amplicon sequencing, using DNA extracted from primary tumors. Tumors are organized into wild type CAST KP which did not receive the sgRNA for *Atrx*, CAST KPA* which retain wild type function of *Atrx* after CRISPR/Cas9 editing, and CAST KPA which have loss of function mutations of *Atrx*. Genomic DNA was extracted from fresh frozen tumors, and next generation amplicon sequencing was performed for the site of *Atrx* targeted by CRISPR/Cas9 sgRNA (blue text). Examples of wild-type, non-frameshift (NFS), frameshift (FS), and large deletion (LD) mutation sequences are shown.

(C–E) Immunohistochemical staining of ATRX on FFPE tumor sections from (C) CAST KP, (D) CAST KPA*, and (E) CAST KPA.

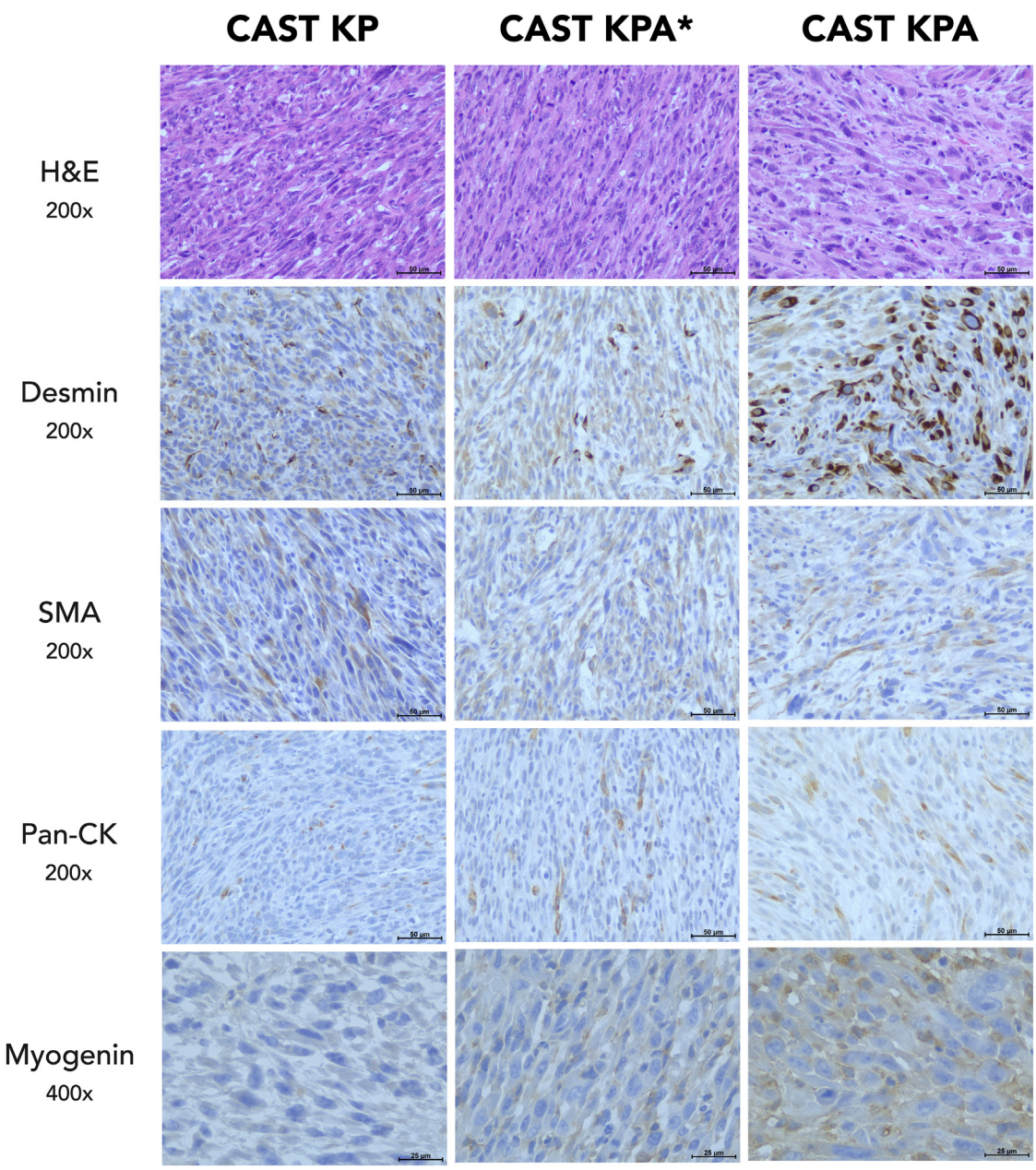

Figure 2. Histological characterization of soft tissue sarcomas

H&E staining and immunohistochemistry of tumors from CAST KP (left), CAST KPA* (middle), and CAST KPA (right). The tumors generated in this model are characterized by focal and patchy staining of desmin, focal staining of smooth muscle actin (SMA), focal staining of pan-cytokeratin (Pan-CK), and negative staining of myogenin.

mTR$^{+/+}$ and mTR$^{+/-}$ tumors, whereas *Atrx* loss did not elevate c-circle quantity to the same degree in mTR$^{-/-}$ tumors (Figure 4C).

In addition to c-circles, ALT positive tumors often have unique nuclear PML bodies which colocalize with telomeres. These ALT-associated PML bodies (APBs) are thought to serve as organizational bodies where the process of telomere maintenance by ALT can occur.[5] We performed immunoFISH on frozen tumor sections to analyze the abundance of APBs in murine sarcoma tissues[33] (Figure 5A). Following imaging, we used a previously established method of analysis to quantify the proportion of APB positive nuclei in each tumor.[34] There was a significant increase in the percentage of nuclei containing APBs in the CAST KPA tumors compared to CAST KP tumors (Figure 5B). Additionally, APBs were observed in CAST KPA tumors from mTR$^{+/+}$, mTR$^{+/-}$, and mTR$^{-/-}$ groups (Figure 5C).

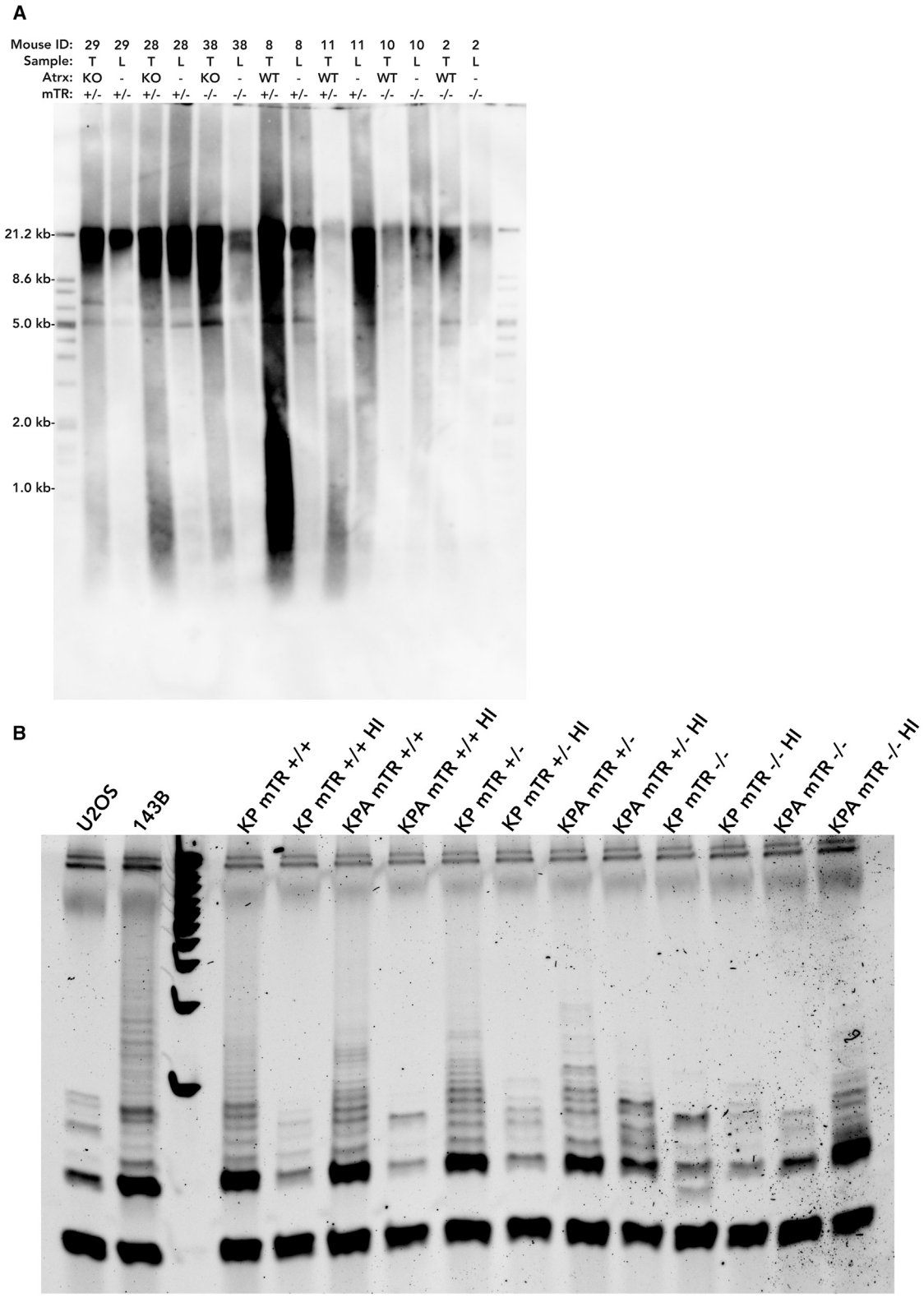

(legend on next page)

Metaphase analysis of primary tumor cells

To determine the effect of loss of *Atrx* expression on chromosome structure and telomere phenotypes, we performed metaphase telomere FISH on a panel of primary cell lines derived from CAST KP and CAST KPA tumors with each mTR genotype: $mTR^{+/+}$, $mTR^{+/-}$, and $mTR^{-/-}$ (Figures 6A and 6B). We quantified fragile telomeres (Figure 6C), undetectable telomeres (Figure 6D), and chromosome fusions (Figure 6E). We observed that $mTR^{-/-}$ cells had an increase in undetectable telomeres at the end of chromosomes (Figure 6F). In primary cell lines with loss of function of *Atrx*, there was an increase in fragile telomeres (Figure 6G). Additionally, in metaphases from cells with loss of both telomerase and *Atrx*, there was an increase in chromosomal fusions compared to cells with loss of telomerase alone (Figure 6H). Importantly, fragile telomeres and chromosome fusions are often signs of chromosomal instability.[35]

To further measure the telomere length distribution in each cell line, we performed quantitative FISH (Q-FISH). To analyze the fluorescent intensity of telomere foci, we used the program TFL-Telo to predict relative telomere length.[36] With partial and complete loss of mTR, telomeres had lower fluorescent intensity (Figure 6I). To quantify the number of telomere sister chromatid exchanges (tSCE) in each cell line, we performed chromosome orientation telomere FISH (CO-FISH) (Figures 7A and 7B). Comparing normal staining (Figure 7C) with tSCE events (Figure 7D), we found a significant increase in tSCE in cell lines derived from tumors with loss of function of *Atrx* with either reduced mTR expression or complete loss of mTR expression compared to *Atrx* wild type cell lines with similar mTR expression. However, we did not observe a difference in tSCE in $mTR^{+/+}$ cell lines with or without functional *Atrx* (Figure 7E).

DISCUSSION

Despite the prevalence of ALT in 10–15% of human cancers, the genomic determinants and specific mechanisms of ALT remain unknown. The lack of ALT positive autochthonous preclinical models is a key constraint that limits the ability to elucidate these mechanisms to develop targeted therapies for cancers with the ALT pathway and to investigate the activation of ALT in an immune competent context. Previous *in vitro* work using E14 mouse embryonic stem cells without mTR showed that these cells can proliferate for many population doublings before entering telomere crisis and inducing the ALT pathway.[37] While these cells have been shown to extend their telomeres using a template known as mTALT, they do not demonstrate production of c-circles or formation of ALT-associated PML bodies, which are characteristic of human ALT positive cancer cells.[37]

In this study, we describe a spatially and temporally restricted primary mouse model of sarcoma that displays multiple molecular phenotypes associated with ALT. The generation of tumors in CAST/EiJ mice, with and without telomerase function, using CRISPR/Cas9 to induce oncogenic $Kras^{G12D}$ and loss of function of both *Trp53* and *Atrx* leads to sarcomagenesis and a subset of tumors which had elevated c-circle production and an increase in the abundance of APB formation. Interestingly, we observed that telomeric c-circles and APBs trended toward higher abundance in Atrx-deficient tumors with intact telomerase activity versus Atrx-deficient tumors that were telomerase deficient (Figures 4C and 5C). The mechanisms underlying this observation remain unclear. However, one possibility is that telomeres shorten rapidly in this model in the $mTR^{-/-}$ condition, thus limiting the genomic substrates upon which break-induced telomere replication can act in the context of Atrx-deficiency.

While the loss of ATRX has been correlated with activation of ALT in human cancers, this study demonstrates a causal relationship between the loss of *Atrx* and the induction of ALT-associated biomarkers, including c-circles, APBs, and tSCE events. While these biomarkers tended to be higher in Atrx-deficient tumors, they did not correlate with the activation of productive telomere length maintenance in the absence of telomerase in Atrx-deficient tumors. This observation suggests that Atrx loss is not sufficient to activate telomere lengthening in this genetically engineered murine sarcoma model, consistent with previous findings suggesting that additional genetic and epigenetic mechanisms may be required after loss of ATRX to induce telomere lengthening by ALT.[16] Another possible explanation for the lack of telomere lengthening in Atrx-deficient tumors without telomerase is that the phenotypes observed in this model are associated with non-productive telomere synthesis.[38] Future studies are needed to determine how productive telomere synthesis by ALT is activated. Our results suggest that other mechanisms, independent of *Atrx* loss, contribute to the activation of ALT-mediated telomere length maintenance *in vivo*. Importantly, the mouse model generated in this study will serve as a useful platform for future *in vivo* studies elucidating additional determinants of ALT.

While previous studies have shown that telomerase expression may repress the activation and function of ALT, recent evidence has demonstrated the co-occurrence of multiple telomere maintenance mechanisms in human cancer.[16,18] The CAST KP and CAST KPA mouse models provide additional evidence that ALT-associated biomarkers can be observed in tumors with functional telomerase activity. Although Atrx knockout did not result in productive telomere lengthening in this model, it did produce multiple traditional ALT phenotypes and markers of telomeric instability which were observed in both telomerase deficient and telomerase proficient tumors. Specifically, the presence of functional telomerase did not affect the production of c-circles, the formation of APBs, or telomere fragility in these tumors. These results indicate that while telomerase may mask some phenotypes of ALT such as the measurement of telomere length distribution, other characteristic markers of ALT such as the presence of c-circles and APBs should be measured

Figure 3. Characterizing telomere length and telomerase function

(A) Telomere restriction fragment assay of RsaI and HinfI restricted DNA from tumors "T" and normal liver controls "L" visualized using chemiluminescent detection.

(B) Telomerase Repeated Amplification Protocol (TRAP) assay performed on cell lines derived from primary tumors. 143B is an osteosarcoma cell line with known telomerase activity (positive control), and U2OS is an osteosarcoma cell line without functional telomerase (negative control).

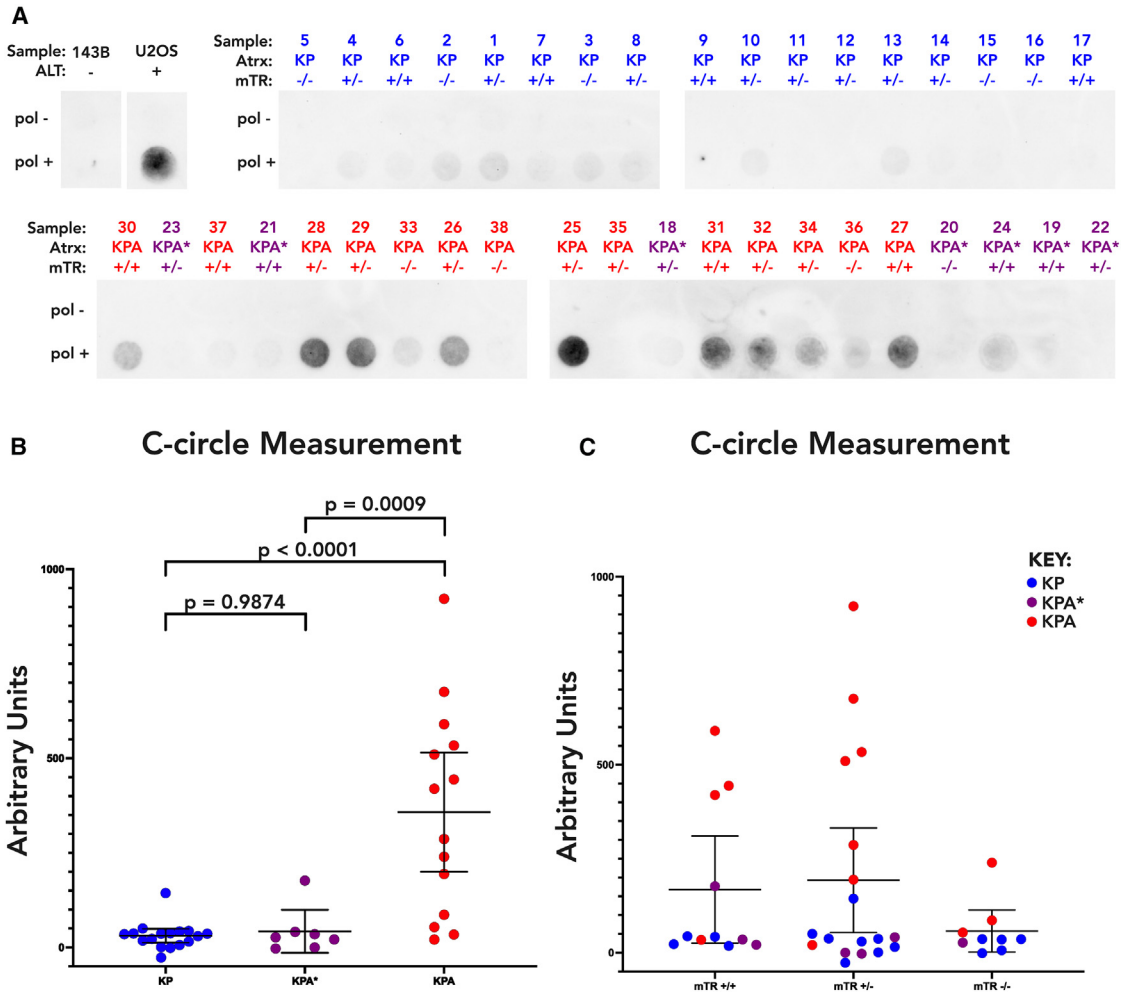

Figure 4. C-circle measurement in primary tumors

(A) Rolling circle amplification of c-circles was performed using DNA extracted from fresh frozen tumors. Chemiluminescent detection of dot blot products from CAST KP (blue), CAST KPA* (purple), and CAST KPA (red) and human control cell lines (black), with and without the addition of phi29 DNA polymerase.

(B) Graphical representation of the average c-circle content of tumors by tumor mutation profile using a one-way ANOVA with Tukey's modification, and error bars are represented as the mean ±95% confidence interval.

(C) Graphical representation of the average c-circle content of tumors by mTR genotype with CAST KP, with error bars represented as the mean ±95% confidence interval (blue), CAST KPA* (purple), and CAST KPA (red).

independently of telomerase status as they should not be assumed to be reliably inferred from telomerase status alone.

One key area for future investigation in this field will be to fully define the mechanism and co-determinants which enable ALT activation in *Atrx*-deficient tumors *in vivo*. While we predict that the loss of epigenetic regulation of telomeres by *Atrx* leads to increased telomere replication stress and DNA damage that is thought to promote break-induced telomere replication, future studies will be needed to precisely delineate the mechanisms and timing by which the loss of *Atrx* contributes to activation of the ALT pathway. While the majority of tumors in this model with loss of function of *Atrx* activated ALT-associated biomarkers, a subset of tumors without functional *Atrx* did not display features of ALT, further suggesting that the loss of *Atrx* alone is not sufficient to activate ALT in mouse primary sarcomas.

While telomerase has been challenging to target therapeutically because inhibition of telomerase in normal stem cells leads to toxicity, proteins essential to ALT may be better targets for future treatments as the pathway is exclusive to cancer cells. In mouse xenograft tumors, it has also been reported that anti-telomerase therapy causes cancer regression, followed by tumor recurrence with the development of ALT as a key mechanism of resistance.[39] The prevalence of ALT in cancer and the escape of tumors after telomerase inhibition by gaining ALT function make targeting the ALT pathway an increasingly important area for further research. Therefore, ALT is a promising target for future therapies for many cancer types.

In summary, using a primary mouse model of sarcoma, we demonstrate that the mutation of *Atrx* facilitates the development of primary sarcomas in mice that display multiple molecular

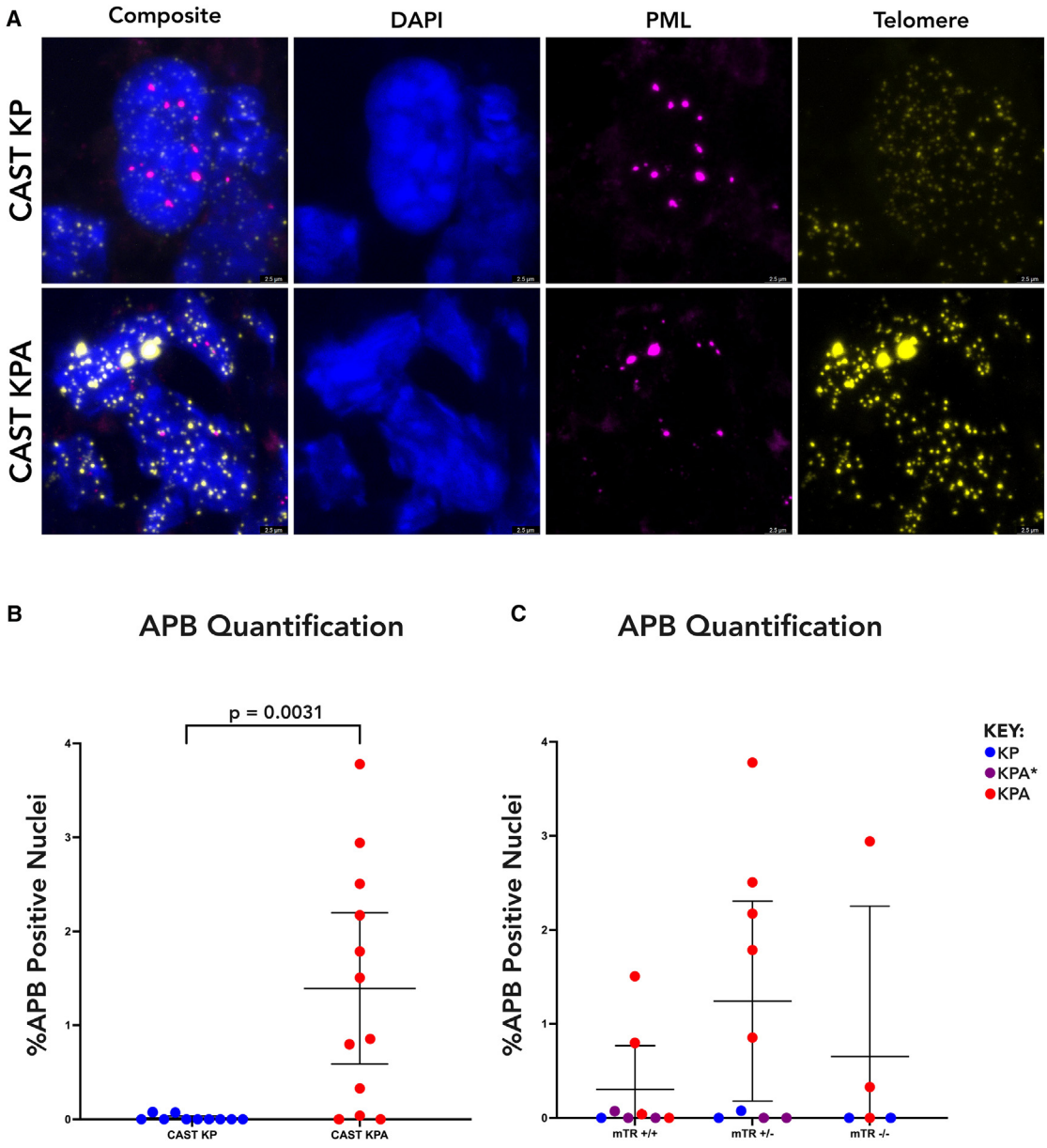

Figure 5. Quantifying ALT-associated PML bodies in primary tumors

(A) Representative images of immunoFISH including DAPI (blue), PML (magenta), and telomere (yellow). The colocalization of ultra-bright telomere foci with PML protein is classified as an ALT-associated PML body (APB). Scale bars have a length of 2.5 um.

(B) Graphical representation of the proportion of APB positive nuclei in individual tumors by *Atrx* mutation status, compared using a Welch's *t* test. Error bars are represented as the mean ±95% confidence interval.

(C) Graphical representation of the proportion of APB positive nuclei by mTR genotype with CAST KP (blue), CAST KPA* (purple), and CAST KPA (red). Error bars are represented as the mean ±95% confidence interval.

markers and phenotypes of ALT. However, Atrx-deficient tumors did not show productive telomere length maintenance in the absence of telomerase, suggesting that other mechanisms are required to maintain telomere length. Nevertheless, the development of this model lays a foundation for future research that may allow for improved understanding of the mechanisms of ALT positive cancer and for testing novel cancer therapies *in vivo*.

Limitations of the study

In this study, we evaluated the extent to which loss of telomerase and *Atrx* contribute to the activation of ALT in a mouse model of sarcoma. Although we observed multiple molecular phenotypes of ALT after loss of function of *Atrx*, we did not observe telomere lengthening in this model. Future studies are needed to elucidate the mechanisms by which loss of *Atrx* leads to molecular

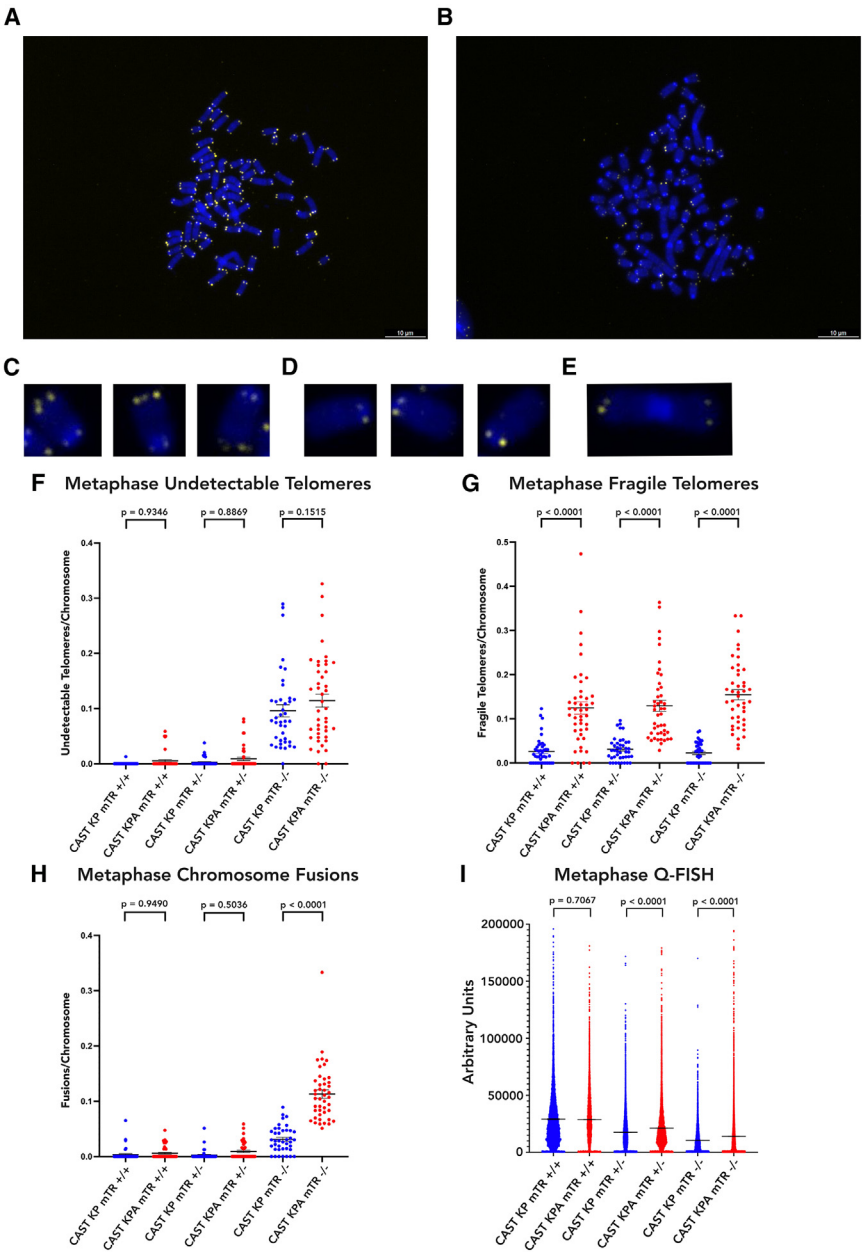

Figure 6. Cytogenetic analysis of primary cell lines

(A) Metaphase Telomere FISH from a CAST KP primary cell line, DAPI (blue) and telomere (yellow).
(B) Metaphase Telomere FISH from a CAST KPA primary cell line. Scale bars have a length of 10um.
(C) Examples of fragile telomeres.
(D) Examples of undetectable telomeres.
(E) Example of chromosome fusion.
(F–I) Graphical representation of (F) undetectable telomeres, (G) fragile telomeres, and (H) chromosome fusions. CAST KP (blue) CAST KPA (red). Statistics performed using one-way ANOVA with Sidak's multiple comparisons. Error bars are represented as the mean ±95% confidence interval (I) Q-FISH violin plot of individual telomere fluorescence values from the TFL-Telo program, compared using a one-way ANOVA with Sidak's multiple comparisons. Error bars are represented as the mean ±95% confidence interval.

phenotypes of ALT, and what additional alterations are required for telomere elongation to occur *in vivo*.

RESOURCE AVAILABILITY

Lead contact

Further information and requests for resources and reagents should be directed to David G. Kirsch (David.Kirsch@uhn.ca).

Materials availability

This study did not generate new unique reagents. Plasmids and cell lines generated are available from the lead contact upon request.

Data and code availability

- All data reported in this paper will be shared by the lead contact upon request.
- This paper does not report original code.
- Any additional information required to reanalyze the data reported in this paper is available from the lead contact upon request.

ACKNOWLEDGMENTS

We thank Dr. Jianguo Huang for providing Rosa26-1loxp-Cas9/+ mice and the Jackson laboratory for providing mTR$^{-/-}$ mice. We thank the STTARR histopathology core for performing H&E and IHC staining. We thank Bill Diplas for advice optimizing the c-circle assay. We thank Dr. Titia de Lange for advice

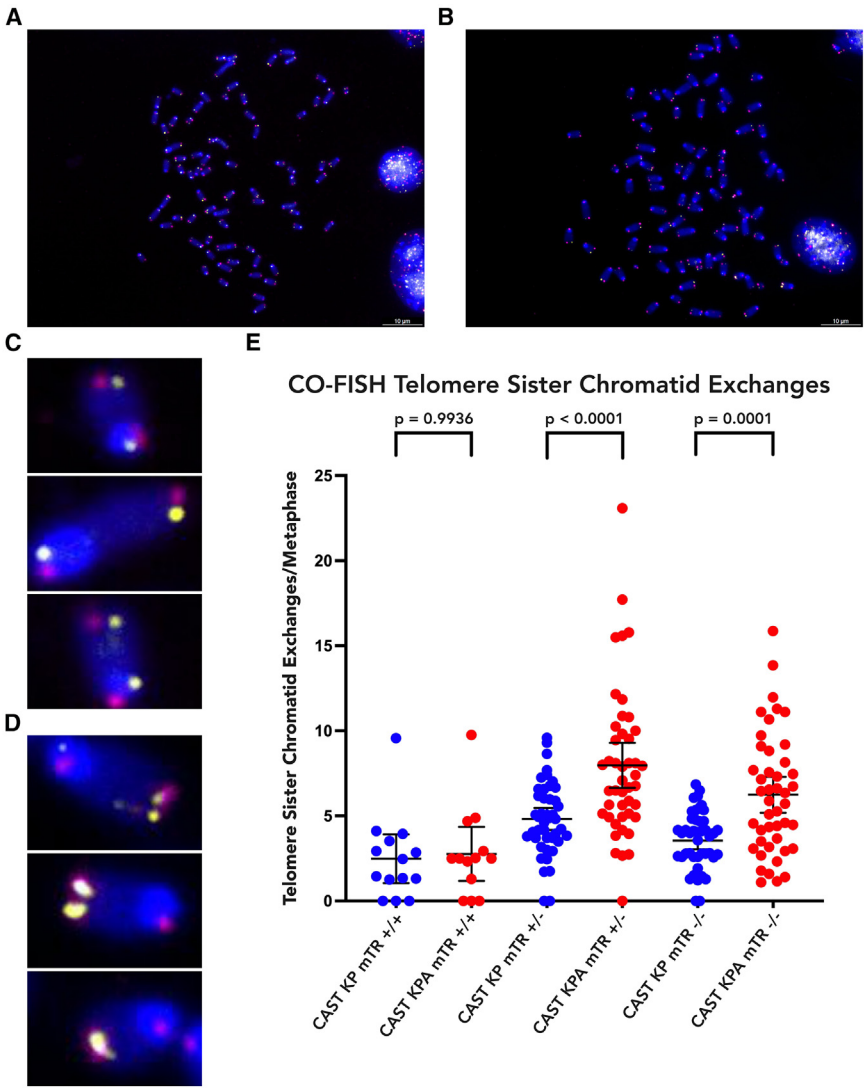

Figure 7. Chromosome orientation FISH (CO-FISH)

(A) Representative image of a CO-FISH metaphase spread (B) Representative image of a CO-FISH metaphase spread with multiple telomere sister chromatid exchanges (tSCE). Scale bars have a length of 10um.

(C) Examples of normal CO-FISH telomere staining.

(D) Examples of CO-FISH telomere staining with tSCE.

(E) Graphical representation of tSCE quantification in each cell line. Statistics performed using a one-way ANOVA with Sidak's multiple comparisons, and error bars are represented as the mean ±95% confidence interval.

interpreting metaphase telomere FISH phenotypes. We thank Dr. Andrea Daniel for advice in experimental design. Graphics for schematics were created using Biorender.com and Inkscape. This work was supported by 7R35CA197616 from the NCI to DGK.

AUTHOR CONTRIBUTIONS

Conceptualization: W.F. and D.G.K.; methodology: M.P., W.F., A.J.W., and D.G.K.; formal analysis: M.P. and W.F.; investigation: M.P., W.F., B.C.D., L.L., and Y.M.; writing–original draft: M.P.; writing–reviewing and editing: M.P., W.F., A.J.W., B.C.D., M.S.W., and D.G.K.; visualization: M.P.; supervision: D.G.K.

DECLARATION OF INTERESTS

D.G.K. is a cofounder of XRad Therapeutics, which is developing radiosensitizers, and serves on the Scientific Advisory Board of Lumicell, which is commercializing intraoperative imaging technology. D.G.K. is a coinventor on patents for radiosensitizers and an intraoperative imaging device. D.G.K. also receives funding for a clinical trial from a Stand Up To Cancer (SU2C) Catalyst Research Grant with support from Merck. The laboratory of D.G.K. currently receives funding or reagents from XRad Therapeutics, Merck, Bristol-Myers Squibb, Varian Medical Systems, and Calithera, but these did not support the research described in this manuscript.

STAR★METHODS

Detailed methods are provided in the online version of this paper and include the following:

- KEY RESOURCES TABLE
- EXPERIMENTAL MODEL AND STUDY PARTICIPANT DETAILS
- METHOD DETAILS
  - Cell line generation from primary tumors
  - Amplicon sequencing
  - C-circle assay
  - ImmunoFISH
  - Metaphase telomere FISH
  - Q-FISH
  - CO-FISH
  - Telomere restriction fragment assay (TRF)
  - Telomerase repeated amplification protocol (TRAP assay)
  - Western blotting
- QUANTIFICATION AND STATISTICAL ANALYSIS

SUPPLEMENTAL INFORMATION

Supplemental information can be found online at https://doi.org/10.1016/j.isci.2025.112357.

Received: December 5, 2023
Revised: July 2, 2024
Accepted: April 1, 2025
Published: April 3, 2025

REFERENCES

1. Szostak, J.W., and Blackburn, E.H. (1982). Cloning yeast telomeres on linear plasmid vectors. Cell *29*, 245–255.
2. Bodnar, A.G., Ouellette, M., Frolkis, M., Holt, S.E., Chiu, C.P., Morin, G.B., Harley, C.B., Shay, J.W., Lichtsteiner, S., and Wright, W.E. (1998). Extension of life-span by introduction of telomerase into normal human cells. Science *279*, 349–352.
3. Shay, J.W., and Bacchetti, S. (1997). A survey of telomerase activity in human cancer. Eur. J. Cancer *33*, 787–791.
4. Bryan, T.M., Englezou, A., Dalla-Pozza, L., Dunham, M.A., and Reddel, R.R. (1997). Evidence for an alternative mechanism for maintaining telomere length in human tumors and tumor-derived cell lines. Nat. Med. *3*, 1271–1274.
5. Yeager, T.R., Neumann, A.A., Englezou, A., Huschtscha, L.I., Noble, J.R., and Reddel, R.R. (1999). Telomerase-negative immortalized human cells contain a novel type of promyelocytic leukemia (PML) body. Cancer Res. *59*, 4175–4179.
6. Henson, J.D., Cao, Y., Huschtscha, L.I., Chang, A.C., Au, A.Y.M., Pickett, H.A., and Reddel, R.R. (2009). DNA C-circles are specific and quantifiable markers of alternative-lengthening-of-telomeres activity. Nat. Biotechnol. *27*, 1181–1185.
7. Londoño-Vallejo, J.A., Der-Sarkissian, H., Cazes, L., Bacchetti, S., and Reddel, R.R. (2004). Alternative lengthening of telomeres is characterized by high rates of telomeric exchange. Cancer Res. *64*, 2324–2327.
8. Heaphy, C.M., Subhawong, A.P., Hong, S.M., Goggins, M.G., Montgomery, E.A., Gabrielson, E., Netto, G.J., Epstein, J.I., Lotan, T.L., Westra, W.H., et al. (2011). Prevalence of the alternative lengthening of telomeres telomere maintenance mechanism in human cancer subtypes. Am. J. Pathol. *179*, 1608–1615.
9. Chudasama, P., Mughal, S.S., Sanders, M.A., Hübschmann, D., Chung, I., Deeg, K.I., Wong, S.H., Rabe, S., Hlevnjak, M., Zapatka, M., et al. (2018). Integrative genomic and transcriptomic analysis of leiomyosarcoma. Nat. Commun. *9*, 144.
10. Liau, J.-Y., Lee, J.C., Tsai, J.H., Yang, C.Y., Liu, T.L., Ke, Z.L., Hsu, H.H., and Jeng, Y.M. (2015). Comprehensive screening of alternative lengthening of telomeres phenotype and loss of ATRX expression in sarcomas. Mod. Pathol. *28*, 1545–1554.
11. Lee, J.-C., Jeng, Y.M., Liau, J.Y., Tsai, J.H., Hsu, H.H., and Yang, C.Y. (2015). Alternative lengthening of telomeres and loss of ATRX are frequent events in pleomorphic and dedifferentiated liposarcomas. Mod. Pathol. *28*, 1064–1073.
12. Ulaner, G.A., Hoffman, A.R., Otero, J., Huang, H.Y., Zhao, Z., Mazumdar, M., Gorlick, R., Meyers, P., Healey, J.H., and Ladanyi, M. (2004). Divergent patterns of telomere maintenance mechanisms among human sarcomas: sharply contrasting prevalence of the alternative lengthening of telomeres mechanism in Ewing's sarcomas and osteosarcomas. Genes Chromosomes Cancer *41*, 155–162.
13. Lovejoy, C.A., Li, W., Reisenweber, S., Thongthip, S., Bruno, J., de Lange, T., De, S., Petrini, J.H.J., Sung, P.A., Jasin, M., et al. (2012). Loss of ATRX, genome instability, and an altered DNA damage response are hallmarks of the alternative lengthening of telomeres pathway. PLoS Genet. *8*, e1002772.
14. Lawlor, R.T., Veronese, N., Pea, A., Nottegar, A., Smith, L., Pilati, C., Demurtas, J., Fassan, M., Cheng, L., and Luchini, C. (2019). Alternative lengthening of telomeres (ALT) influences survival in soft tissue sarcomas: a systematic review with meta-analysis. BMC Cancer *19*, 232–237.
15. Li, F., Deng, Z., Zhang, L., Wu, C., Jin, Y., Hwang, I., Vladimirova, O., Xu, L., Yang, L., Lu, B., et al. (2019). ATRX loss induces telomere dysfunction and necessitates induction of alternative lengthening of telomeres during human cell immortalization. EMBO J. *38*, e96659.
16. Turkalo, T.K., Maffia, A., Schabort, J.J., Regalado, S.G., Bhakta, M., Blanchette, M., Spierings, D.C.J., Lansdorp, P.M., and Hockemeyer, D. (2023). A non-genetic switch triggers alternative telomere lengthening and cellular immortalization in ATRX deficient cells. Nat. Commun. *14*, 939.
17. Graham, M.K., Kim, J., Da, J., Brosnan-Cashman, J.A., Rizzo, A., Baena Del Valle, J.A., Chia, L., Rubenstein, M., Davis, C., Zheng, Q., et al. (2019). Functional Loss of ATRX and TERC Activates Alternative Lengthening of Telomeres (ALT) in LAPC4 Prostate Cancer Cells Effects of ATRX and hTR Loss in Prostate Cancer. Mol. Cancer Res. *17*, 2480–2491.
18. Brosnan-Cashman, J.A., Yuan, M., Graham, M.K., Rizzo, A.J., Myers, K.M., Davis, C., Zhang, R., Esopi, D.M., Raabe, E.H., Eberhart, C.G., et al. (2018). ATRX loss induces multiple hallmarks of the alternative lengthening of telomeres (ALT) phenotype in human glioma cell lines in a cell line-specific manner. PLoS One *13*, e0204159.
19. Clynes, D., Jelinska, C., Xella, B., Ayyub, H., Scott, C., Mitson, M., Taylor, S., Higgs, D.R., and Gibbons, R.J. (2015). Suppression of the alternative lengthening of telomere pathway by the chromatin remodelling factor ATRX. Nat. Commun. *6*, 7538.
20. Napier, C.E., Huschtscha, L.I., Harvey, A., Bower, K., Noble, J.R., Hendrickson, E.A., and Reddel, R.R. (2015). ATRX represses alternative lengthening of telomeres. Oncotarget *6*, 16543–16558.
21. Lovejoy, C.A., Takai, K., Huh, M.S., Picketts, D.J., and de Lange, T. (2020). ATRX affects the repair of telomeric DSBs by promoting cohesion and a DAXX-dependent activity. PLoS Biol. *18*, e3000594.
22. Watson, L.A., Solomon, L.A., Li, J.R., Jiang, Y., Edwards, M., Shin-ya, K., Beier, F., and Bérubé, N.G. (2013). Atrx deficiency induces telomere dysfunction, endocrine defects, and reduced life span. J. Clin. Investig. *123*, 2049–2063.
23. de Nonneville, A., Salas, S., Bertucci, F., Sobinoff, A.P., Adélaïde, J., Guille, A., Finetti, P., Noble, J.R., Churikov, D., Chaffanet, M., et al. (2022). TOP3A amplification and ATRX inactivation are mutually exclusive events in pediatric osteosarcomas using ALT. EMBO Mol. Med. *14*, e15859.
24. Prowse, K.R., and Greider, C.W. (1995). Developmental and tissue-specific regulation of mouse telomerase and telomere length. Proc. Natl. Acad. Sci. USA *92*, 4818–4822.
25. Blasco, M.A., Lee, H.W., Hande, M.P., Samper, E., Lansdorp, P.M., DePinho, R.A., and Greider, C.W. (1997). Telomere shortening and tumor formation by mouse cells lacking telomerase RNA. Cell *91*, 25–34.
26. Hemann, M.T., and Greider, C.W. (2000). Wild-derived inbred mouse strains have short telomeres. Nucleic Acids Res. *28*, 4474–4478.
27. Strong, M.A., Vidal-Cardenas, S.L., Karim, B., Yu, H., Guo, N., and Greider, C.W. (2011). Phenotypes in mTERT+/− and mTERT−/− mice are due to short telomeres, not telomere-independent functions of telomerase reverse transcriptase. Mol. Cell Biol. *31*, 2369–2379.
28. Morrish, T.A., and Greider, C.W. (2009). Short telomeres initiate telomere recombination in primary and tumor cells. PLoS Genet. *5*, e1000357.
29. Huang, J., Chen, M., Whitley, M.J., Kuo, H.C., Xu, E.S., Walens, A., Mowery, Y.M., Van Mater, D., Eward, W.C., Cardona, D.M., et al. (2017). Generation and comparison of CRISPR-Cas9 and Cre-mediated genetically engineered mouse models of sarcoma. Nat. Commun. *8*, 15999.
30. Floyd, W., Pierpoint, M., Su, C., Patel, R., Luo, L., Deland, K., Wisdom, A.J., Zhu, D., Ma, Y., DeWitt, S.B., et al. (2023). Atrx deletion impairs

CGAS/STING signaling and increases sarcoma response to radiation and oncolytic herpesvirus. J. Clin. Investig. *133*, e149310.

31. Kirsch, D.G., Dinulescu, D.M., Miller, J.B., Grimm, J., Santiago, P.M., Young, N.P., Nielsen, G.P., Quade, B.J., Chaber, C.J., Schultz, C.P., et al. (2007). A spatially and temporally restricted mouse model of soft tissue sarcoma. Nat. Med. *13*, 992–997.

32. Hathcock, K.S., Hemann, M.T., Opperman, K.K., Strong, M.A., Greider, C.W., and Hodes, R.J. (2002). Haploinsufficiency of mTR results in defects in telomere elongation. Proc. Natl. Acad. Sci. USA *99*, 3591–3596.

33. Cesare, A.J., Heaphy, C.M., and O'Sullivan, R.J. (2015). Visualization of telomere integrity and function *in vitro* and *in vivo* using immunofluorescence techniques. Curr. Protoc. Cytom. *73*, 12–40.

34. Henson, J.D., Hannay, J.A., McCarthy, S.W., Royds, J.A., Yeager, T.R., Robinson, R.A., Wharton, S.B., Jellinek, D.A., Arbuckle, S.M., Yoo, J., et al. (2005). A robust assay for alternative lengthening of telomeres in tumors shows the significance of alternative lengthening of telomeres in sarcomas and astrocytomas. Clin. Cancer Res. *11*, 217–225.

35. Koschmann, C., Calinescu, A.A., Nunez, F.J., Mackay, A., Fazal-Salom, J., Thomas, D., Mendez, F., Kamran, N., Dzaman, M., Mulpuri, L., et al. (2016). ATRX loss promotes tumor growth and impairs nonhomologous end joining DNA repair in glioma. Sci. Transl. Med. *8*, 328ra28.

36. Poon, S.S., Martens, U.M., Ward, R.K., and Lansdorp, P.M. (1999). Telomere length measurements using digital fluorescence microscopy. Cytometry *36*, 267–278.

37. Niida, H., Shinkai, Y., Hande, M.P., Matsumoto, T., Takehara, S., Tachibana, M., Oshimura, M., Lansdorp, P.M., and Furuichi, Y. (2000). Telomere maintenance in telomerase-deficient mouse embryonic stem cells: characterization of an amplified telomeric DNA. Mol. Cell Biol. *20*, 4115–4127.

38. Lu, R., Nelson, C.B., Rogers, S., Cesare, A.J., Sobinoff, A.P., and Pickett, H.A. (2024). Distinct modes of telomere synthesis and extension contribute to Alternative Lengthening of Telomeres. iScience *27*, 108655.

39. Hu, J., Hwang, S.S., Liesa, M., Gan, B., Sahin, E., Jaskelioff, M., Ding, Z., Ying, H., Boutin, A.T., Zhang, H., et al. (2012). Antitelomerase therapy provokes ALT and mitochondrial adaptive mechanisms in cancer. Cell *148*, 651–663.

STAR★METHODS

KEY RESOURCES TABLE

REAGENT or RESOURCE	SOURCE	IDENTIFIER
Antibodies		
ATRX Rabbit pAB	Abcam	ab97508; RRID:AB_10680289
Anti-PML Antibody clone 36.1-104	Millipore Sigma	05-718; RRID:AB_11213854
Goat anti-Mouse IgG (H+L) Cross-Adsorbed Secondary Antibody, Alexa Fluor™ 647	Invitrogen	A-21235; RRID:AB_2535804
IRDye® 800CW Goat anti-Rabbit IgG Secondary Antibody	LicorBio	926-32211; RRID:AB_621843
Chemicals, peptides, and recombinant proteins		
RNAse A	Thermofischer	EN0531
Colcemid	Thermofischer	15212012
Accuprime Taq Polymerase	Thermofischer	12339016
Qiagen Protease	Qiagen	19157
Phi 29 Polymerase	NEB	M0269
Prolong Glass Antifade with DAPI	Thermofischer	P36984
Intercept® (TBS) Protein-Free Blocking Buffer	LicorBio	927-80001
SYBR™ Safe DNA Gel Stain	Thermofischer	S33102
Exonuclease III	NEB	M0206
Critical commercial assays		
DNeasy Blood and Tissue Kit	Qiagen	69504
Puregene Tissue Kit	Qiagen	158063
Qubit 1X dsDNA HS Assay Kit	ThermoFischer	Q33230
BCA Protein Assay Kit	ThermoFischer	A65453
*Telo*TAGGG™ Telomere Length Assay	Roche	12209136001
TRAPeze® Telomerase Detection Kit	Millipore Sigma	S7700
Experimental models: Cell lines		
U-2 OS (HTB-96)	ATCC	U2OS
143B (CRL-8303)	ATCC	143B
Experimental models: Organisms/strains		
CAST/EiJ	Jackson Labs	Strain 000928
B6.Cg-*Terc*^{tm1Rdp}/J	Jackson Labs	Strain 004132
Rosa26-1loxp-Cas9	Bred in Lab	N/A
CAST/EiJ Rosa26-1loxp-Cas9	Bred in Lab	CAST mTR +/+
CAST/EiJ Rosa26-1loxp-Cas9 mTR +/−	Bred in Lab	CAST mTR +/−
CAST/EiJ Rosa26-1loxp-Cas9 mTR −/−	Bred in Lab	CAST mTR −/−
Oligonucleotides		
Atrx Exon 8a F	IDT	GAG ACG GCA ACA GTG GGA CT
Atrx Econ 8a R	IDT	ACA TTG CAG GGT TGC TTT CTG
TelC-Cy3 (Telomere FISH probe)	PNA Bio	F1002
TelG-Alexa488 (Telomere FISH probe)	PNA Bio	F1008
Recombinant DNA		
KPS Kras HDR template Kras gRNA	GenScript	Kras
p53 gRNA only AAV Px552 backbone	GenScript	p53
p53 gRNA atrx 8a gRNA Px552 backbone	GenScript	p53+Atrx
Software and algorithms		
Graphpad Prism v. 9.0	Graphpad	Graphpad Prism v. 9.0

(*Continued on next page*)

Continued

REAGENT or RESOURCE	SOURCE	IDENTIFIER
LAS X	Leica	LAS X
Image J	NIH Image	Image J
Biorender Image Editing	Biorender.com	Biorender
Inkscape	Inkscape.com	Inkscape
TFL-Telo	TFL-Telo	TFL-Telo

EXPERIMENTAL MODEL AND STUDY PARTICIPANT DETAILS

Mice of mixed background (129SVJ/C57/Bl6) with Rosa26-1loxp-Cas9 and with mTR$^{-/-}$ (B6.Cg-*Terc*^{tm1Rdp}/J; Jackson Labs 004132) were crossed with CAST/EiJ mice from Jackson labs (Strain 000928). The mice generated from these crosses were then bred on a pure CAST/EiJ background for at least five generations. Genotyping was performed by Transnetyx using mouse tails to assess Rosa26-1loxp-Cas9 and mTR genotypes. After five generations, using littermate controls, both male and female mice were injected with either KP or KPA plasmids reconstituted at 1ug/ml in half normal saline into the gastrocnemius of the right hind limb using electroporation set at 100V. Plasmids were ordered from Genscript. Mice were checked for tumors after 60 days. All animal studies were approved by the IACUC at Duke University. The sequences for sgRNA are as follows: *Kras* sgRNA: TACGATAGAGGTAACGCTGC, *Trp53* sgRNA: GTGTAATAGCTCCTGCATGG, *Atrx* sgRNA: CCCCAGAACTTTTACGGCC. The sequence for *Kras*^{G12D} HDR is: TGAGAAGTGGACTTTCTTTCTCTGTGGTGAGCTCTCATGAGAAGTGGACTTTCTTGCACCTATGGTTCCCTAACACCCAGTTTAAAG CCTTGGAACTAAAGGACATCACATATAACTGAAATAACTTTCAATATAATTTTCTAATAAATATAAAAATGATATCTTTTTCAAAGCGG CTGGCTGCCGTCCTTTACAAGCGCACGCAGACTGTAGAGCAGCGTTACCTCGATGGTTGGATCATACTCATCCACAAAGTGATTC TGAATTAGCTGTATCGTCAAAGCGCTCTTGCCCACGCCGTCGGCGCCCACGACCACAAGTTTATACTCAGTCATTTTCAGCAGGC CTTACAATAAAAATAATAAAATACAACTAAATTAGAACATGTCTCACACAAGATTATCAAAAACTTTATCAATATTTTAACACTCACCTT TGTGTGTAAAACTCTAAGATATTCCGAATTCAGTGACTACAGATGTACAGAGTAACCTGTAAGTCACTTACAACTTTCTCATCAACAC TTAATAAAAATACATGGAAACCAGTACTTTCATCTTCTATCATTTAGCTTGTTGATCTAAACAGCCAGATTACTGTTTTGTAGCAGCTA ATGGCTCTCAAAGGAATGTATCATGACTTCACTCAGTACAAATATTCTGCATAGTACGCTATACCCTGTGGACACACCCGCATGAG CTTGTCGACAGCTATCCCAACACCTACCCTTGCGGTATTCTTTGTTGACTGGATATTAAAAGTTAGAAGTTAGGTAGCCTAAGAACA TCTGTGTTGGAGCCA. Human cell lines used in this study include 143B and U2OS, and they were acquired from ATCC. The 143B and U2OS Cell lines were not authenticated or tested for mycoplasma.

METHOD DETAILS

Cell line generation from primary tumors

After reaching growth endpoint, tumors were collected from sacrificed mice and digested in dissociation buffer in PBS containing Collagenase Type IV, dispase, and trypsin. Cells were washed in PBS and filtered using a 40um sieve before culture. After five passages, cells were frozen for use in experiments.

Amplicon sequencing

Fresh frozen tumors embedded in OCT from CAST KP and CAST KPA mice were cut into 50um slices and stored in Eppendorf Tubes at –20°C. To prepare tumor tissue for DNA extraction, 1mL of cold PBS was added to each sample on ice. Then, tubes were spun down and residual PBS with dissolved OCT was removed. DNA was extracted using Qiagen DNeasy Blood and Tissue kit. 20ng of DNA was aliquoted from each tumor sample and amplified in a Bio-Rad thermocycler for 35 cycles of PCR using AccuPrime Taq Polymerase with the following primers for *Atrx* exon 8a Forward Primer: GAG ACG GCA ACA GTG GGA CT and Reverse Primer: ACA TTG CAG GGT TGC TTT CTG (IDT). PCR products were sequenced by Genewiz using Amplicon-EZ, and sequences were categorized as wild type (no indel), non-frameshift (indel with size divisible by 3 and less than 50), frameshift (indel with size not divisible by 3 and less than 50), or structural variant (indel with size greater than 50) by alignment using the NCBI BLAST tool.

C-circle assay

Fresh frozen tumors embedded in OCT were cut into 20um slices and stored in Eppendorf Tubes at –20°C. To prepare tumor tissue for DNA extraction, 1mL of cold PBS was added to each sample on ice. Then, tubes were spun down and residual PBS with dissolved OCT was removed. DNA was extracted using QCP DNA extraction described previously.[6] While samples and Qiagen protease are placed in ice, QCP lysis buffer is warmed to 56°C. Qiagen protease is added to QCP lysis buffer at a ratio of 1:20, and 50ul of the resulting lysis buffer is added to each tissue sample. Samples were then incubated at 56°C for one hour with periodic vortexing and incubated at 70°C for 20 minutes to inactivate the protease. DNA was quantified using the Qubit HS assay. 1ul containing 40ng of DNA was aliquoted into 9ul of 10mM Tris HCL pH 7.5 in preparation for rolling circle amplification. To perform amplification of c-circles using Phi29 polymerase,

10ul of Master Mix with or without phi29 polymerase was added to each sample and gently mixed. Samples were incubated in a Bio-Rad thermocycler at 30°C for 8 hours, then heat inactivated at 70°C for 20 minutes and stored at 11°C until being collected. 60ul of 2x saline-sodium citrate (SSC) was added to each sample after amplification was complete. To prepare for dot blotting of c-circle products, a nylon membrane was cut to fit the dot blotting apparatus (GE Whatman Minifold I). The nylon membrane and Whatman paper were hydrated in water for 5 minutes, then in 2x SSC for 5 minutes. The nylon membrane was added to the dot blot apparatus on top of Whatman paper, and bubbles were removed from the nylon membrane. To ensure the vacuum was working properly, 100ul of 2x SSC was loaded into each well and the vacuum was turned on. Then, samples were loaded into each well using a multichannel pipette, with 2x SSC added to empty wells, and the vacuum was turned on. Lastly, 100ul of 2x SSC was added to each well and the vacuum was turned on. While the membrane was still moist, it was crosslinked twice at 454 nm for 1200J using the auto crosslink function (Stratagene UV Stratlinker 1800) before preparing for hybridization. Hybridization of the DIG-telomere probe and chemiluminescent detection was performed according to the protocol from the TeloTAGGG Telomere Length Assay (Roche). The nylon membrane was prehybridized in prewarmed DIG Easy Hyb Granules for 60 minutes at 42°C. Next, the membrane was hybridized with the telomere probe for three hours at 42°C. The membrane was then washed and blocked before incubation with the Anti-DIG-AP. After washing and incubation in detection buffer, substrate solution was added to activate chemiluminescence. Images were taken using the Chemidoc MP imaging system and the Image Lab software. Image J was used to quantify each dot blot by first subtracting the background signal then measuring the integrated density of each dot blot product. The integrated density of each no phi control was subtracted from the phi amplified product. The c-circle assay was performed on each tumor sample three times using DNA extracted from unique adjacent frozen slices, and the results of these experiments were averaged. For each experiment, U2OS was included as a positive control, and 143B was included as a negative control. The average c-circle content of tumors from the CAST KP, CAST KPA*, and CAST KPA groups were compared using a one-way ANOVA with Tukey's modification.

ImmunoFISH

This protocol was adapted from previous methods.[32] Briefly, fresh frozen tumors embedded in OCT were cut into 5um slices and mounted to charged slides before being frozen at –80°C. Slides were fixed in ice cold methanol for 20 minutes at –20°C. Slides were then rehydrated using an ethanol series each for 3 minutes at room temperature (100%, 95%, 70%, di H2O). Slides were then washed in 1% Tween 20 for one minute before antigen retrieval using citrate buffer pH 6 by boiling in a rice cooker for 30 - minutes. Slides were then cooled for 10 minutes and washed in di H2O. Slides were then dehydrated in (70%, 95%, 100%) ethanol and allowed to air dry. To each slide, 50ul of PNA probe was added, and samples were denatured at 83°C for 5 minutes. Following this step, slides were protected from light. Slides were incubated in a hybridization chamber for 2 hours at room temperature and subsequently washed in PNA wash buffer 2 x 15 minutes. Slides were washed in PBST 3 x 5 minutes. Then, slides were incubated in primary antibody for PML (1:100 Mouse Anti-PML Antibody, clone 36.1-104) for 45 minutes at room temperature. Next, the slides were washed 3 x 5 minutes in PBST and incubated in secondary antibody (1:100 Goat anti-Mouse IgG Alexa Fluor 647 Cross-absorbed secondary antibody) for 30 minutes at room temperature. Slides were washed 3 x 5 minutes in PBST and once in di H2O before being mounted in Prolong Glass Antifade with DAPI. Slides were stored at room temperature for 24 hours in the dark and one week at 4°C before imaging using the Leica STED confocal microscope. During imaging, 10 tiles from each tumor slide were randomly chosen using DAPI staining as a reference for z-stack imaging. ALT-associated PML bodies were quantified in max intensity projection image by manually counting the colocalization of ultra-bright telomere foci and PML bodies. Image names were randomized for blinded analysis. For each quantified APB, it was confirmed that colocalization occurred on a single z-plane image. The percentage of APB positive nuclei from tumors in the CAST KP/KPA* and CAST KPA groups were compared using a Welch's t-test. Representative images for Figure 4 were taken using the 100x/1.4 HCX PL APO OIL DIC WD 90 um objective with 5x Zoom at 4096x4096 resolution. All immunoFISH images are displayed as maximum intensity projections using ImageJ.

Metaphase telomere FISH

Exponentially growing primary mouse sarcoma cells derived from CAST KP and CAST KPA tumors were incubated in 100ng/mL Colcemid for 1 hour. Cells were then collected using trypsin and incubated in hypotonic solution at 37°C for 8 minutes. Fixative solution was added dropwise, and cells were fixed overnight at 4°C. Cells were then resuspended in fresh fixative solution and metaphase spreads were made on ethanol washed slides. Slides were incubated overnight at room temperature. Slides were washed in PBS before fixation in 4% paraformaldehyde at room temperature for 5 minutes. Slides were then washed in PBS 3 x 5 minutes. Metaphase spreads were treated in 250 ug/mL RNase A for 15 minutes at 37°C in a humidified chamber. Then slides were fixed a second time in 4% paraformaldehyde for 5 minutes at room temperature and washed 3 x 5 minutes in PBS. Slides were dehydrated using an ethanol series (70%, 95%, 100%) and allowed to air dry. Chromosomes were incubated in Tel C Cy 3 PNA probe (PNA Bio) at 83°C for 5 minutes and allowed to hybridize at room temperature in a dark hybridization chamber for 2 hours at room temperature. Slides were washed 2 x 10 minutes in PNA wash A, then 3 x 5 minutes in PNA wash B before a quick wash in di H2O and mounting in Prolong Glass Antifade with DAPI. All fluorescent widefield images were taken using identical settings to allow for comparison. ImageJ was used to quantify fragile telomeres, chromosome fusions, and undetectable telomeres in each metaphase. To compare undetectable telomere, fragile telomere, and chromosome fusion events between CAST KP and CAST KPA cell lines with $mTR^{+/+}$, $mTR^{+/-}$, and $mTR^{-/-}$, a one-way ANOVA was performed with Sidak's multiple comparisons.

Q-FISH

The TFL-Telo program was used to generate brightness estimation of telomeric foci. For each cell line, over 40 metaphases were quantified with over ten metaphases from each of three replicates. The measured telomere brightness between CAST KP and CAST KPA cell lines with $mTR^{+/+}$, $mTR^{+/-}$, and $mTR^{-/-}$ was compared using a one-way ANOVA with Sidak's multiple comparisons.

CO-FISH

Primary mouse sarcoma cells derived from CAST KP and CAST KPA tumors were incubated in 10uM 3:1 BrdU/BrdC in growth media for 12-16 hours (7.5uM BrdU, 2.5uM BrdC). Cells were then incubated in fresh media with 100ng/mL Colcemid for 2 hours. Cells were then collected using trypsin and incubated in hypotonic solution at 37°C for 8 minutes. Fixative solution was added dropwise, and cells were fixed overnight at 4°C. Cells were then resuspended in fresh fixative solution and metaphase spreads were made on ethanol washed slides. Slides were incubated overnight at room temperature. Chromosomes were then washed in PBS and fixed in 2% paraformaldehyde for 10 minutes at room temperature before washing 3 x 5 minutes in PBS. Slides were then washed in 2x SSC and incubated in 2x SSC with 0.5ug /mL Hoechst stain for 15 minutes in the dark. Slides were then exposed to 365nm UV light for 30 minutes using a Stratalinker and washed in di H2O. DNA labeled with BrdU and BrdC was then digested using Exonuclease III at 37°C for 30 minutes. Slides were washed in PBS. Next, DNA was denatured by heating at 70°C for 10 minutes in (70% formamide, 30% 2x SSC). After denaturing, slides were dehydrated using an ethanol series (70%, 95%, 100%) and allowed to air dry. Chromosomes were hybridized to Tel G 488 PNA probe (PNA Bio) and washed in PNA Wash Buffer A before hybridization with Tec C Cy3 PNA probe (PNA Bio) and subsequent washes in PNA Wash A and PNA Wash B. Slides were washed in di H2O and mounted using Prolong Glass Antifade with DAPI. Images were taken using consistent settings on a widefield fluorescent microscope. Telomere sister chromatid exchanges were quantified using signal from the Tel C probe as it was most consistent between cell lines with different telomere lengths, but representative images of both probes are displayed in the figures after consistent gating of background signal from the Tel G probe using ImageJ. The number of tSCE between CAST KP and CAST KPA cell lines with $mTR^{+/+}$, $mTR^{+/-}$, and $mTR^{-/-}$ was compared using a one-way ANOVA with Sidak's multiple comparisons.

Telomere restriction fragment assay (TRF)

Genomic DNA was extracted from mouse tumors and livers using the Puregene Tissue Kit (Qiagen). The TeloTAGGG Telomere Length Assay kit (Roche) was used to perform southern blotting of telomeres from each sample. Briefly, 2ug of DNA from each sample was restricted with RsaI and HinfI then loaded onto a gel for electrophoresis. DNA was transferred from the gel to a nylon membrane using southern blotting by capillary action overnight. The membrane was crosslinked twice at 454 nm for 1200J using the auto crosslink function (Stratagene UV Stratlinker 1800) before hybridization of the DIG-telomere probe and chemiluminescent detection was performed. Images were taken using the Chemidoc MP imaging system and the Image Lab software.

Telomerase repeated amplification protocol (TRAP assay)

Telomerase activity was assayed in primary cell lines using the TRAPeze Telomerase Detection Kit (Roche). First, $1x10^5$ cells were collected from each cell line and resuspended in 1x CHAPS Lysis Buffer on ice for 30 minutes. Samples were spun down, and protein was measured in each sample using the BCA assay. The PCR reaction was set up according to the TRAPeze protocol, and products were separated on a 10x TBE gel before detection using SYBR Safe and imaging by the Chemidoc MP imaging system. 143B cells were included as a positive control, and U2OS cells were included as a negative control. Heat-inactivated controls were included for experimental samples as internal negative controls. Notably, Primer-Dimer PCR artifacts were observed in the samples, leading to extra bands at less than 100 bp in telomerase negative samples and heat-inactivated samples. Telomerase function was predicted by observing the presence of amplified products above 100 bp.

Western blotting

Cell lines were lysed for 30 minutes on ice in RIPA buffer containing proteinase inhibitor, phosphatase inhibitor, and aproteinin then centrifuged at 10,000g for 10 minutes at 4°C. The BCA assay was performed to measure protein concentration, and samples were diluted to similar concentrations before being boiled in 4x Laemmli sample buffer. Samples were run using a 4-20% Tris-glycine polyacrylamide gel and transferred overnight at 4°C. Membranes were blocked in 1:1 TBS:Intercept blocking buffer for 1 hour before incubation overnight in primary antibody at 4°C (Abcam ab97508). After washing in 0.1% TBS-T, the membrane was incubated with goat anti-rabbit IRDye800 in 0.1% TBS-T (1:10,000) for 1 hour at room temperature. The membrane was washed in 0.1% TBS-T and imaged using an Odyssey CLx.

QUANTIFICATION AND STATISTICAL ANALYSIS

Prism 9 (GraphPad Software Inc.) was used for statistical analysis, and descriptions of tests performed can be found in the figure legends. For graphical representation, all data is presented as the mean ± 95% confidence interval. A *P* value of less than 0.05 indicated significance.